Journal of Cleaner Production xxx (xxxx) xxx

Contents lists available at ScienceDirect

Journal of Cleaner Production

journal homepage: www.elsevier.com/locate/jclepro

Impact of agro-industrial waste on steel corrosion susceptibility in media simulating concrete pore solutions

Murilo F. Gromboni [a], Almir Sales [b, *], Mariana de A.M. Rezende [b], Juliana P. Moretti [b, c], Patricia G. Corradini [a], Lucia H. Mascaro [a]

[a] Department of Chemistry, Federal University of São Carlos, Via Washington Luiz, Km 235, CEP 13565-905, São Carlos, SP, Brazil
[b] Department of Civil Engineering, Federal University of São Carlos, Via Washington Luis, km 235, São Carlos, SP, 13565-905, Brazil
[c] Sea Institute, Federal University of São Paulo, Dr. Carvalho de Mendonça St, 144, Santos, SP, 11070-102, Brazil

ARTICLE INFO

Article history:
Received 29 November 2019
Received in revised form
3 September 2020
Accepted 12 October 2020
Available online xxx

Handling editor. Yutao Wang

Keywords:
Sugarcane bagasse ash sand (SBAS)
Concrete pore solution
Environment-friendly concrete
Corrosion inhibitor
Electrochemical impedance spectroscopy

ABSTRACT

Sugarcane bagasse ash sand (SBAS) can be used as a bioadditive in concrete. However, little is known about its effects on the steel corrosion process. This paper reports the evaluation of the corrosion susceptibilities of steel immersed in simulate concrete pore solutions, with addition of SBAS, to understand the corrosion process in reinforced structure. The open-circuit potential profiles and polarisation curves suggested the favourable formation of a passive film on the steel immersed in the SBAS-containing medium. Electrochemical impedance spectroscopy confirmed that the SBAS-containing medium presents better passivating properties, showing that this recycled material can be used as corrosion inhibitor for reinforced concrete, encouraging its use in the civil industry.

1. Introduction

To realise economy decarbonisation in Brazil, the sugarcane industry has been stimulated following the increasing demands for ethanol, which is largely used in the country as a biofuel. Worldwide, the sugarcane crop has increased by 23.3% since 2009, and Brazil, India, and Thailand reported record production outputs in 2017 (USDA, 2017). As the largest sugarcane producer in the world, Brazil harvested 665.6 million tons of sugarcane in 2016 (Farias and Costa, 2018). However, the entire sugar and ethanol manufacturing framework generates high amounts of waste every year, with major concerns regarding the appropriate disposal and/or re-utilisation of these residues.

The direct residue from sugarcane milling is bagasse, which is mainly burned in incinerators to produce heat and electricity that are fed back to the processing plant. As the final waste from the burning process, approximately 4 million tons of sugarcane bagasse ash sand (SBAS) was generated in 2016 (de Souza, 2017; Farias and Costa, 2018). Environmentally friendly solutions have been proposed for the strategic utilisation of SBAS, such as its use as an additive in different composites, where it is known to produce enhanced mechanical properties in the final bio-material (Anupam et al., 2013; Ozório et al., 2015; Santos et al., 2014). To the best of our knowledge, our research group is the first to propose a particular interesting destination for SBAS, which is the application of such waste as a fine aggregate in mortars, leading to an efficient way to replace natural sand in the formulation of concrete, and ultimately reducing the macro pores (Moretti et al., 2018), enhancing its mechanical, and other physical properties (Almeida et al., 2015; Lima et al., 2011; Moretti et al., 2016).

In addition to their physical and mechanical properties, another aspect of greener concretes that should be studied is their susceptibility to corrosion. Reinforcement corrosion, which has been widely reported in the literature over the last two to three decades, has been studied from different perspectives and considering several factors such as the chloride exposure, carbonation, gas penetration, and concrete ingredients (Ahmad, 2003; Hornbostel et al., 2013; Liu et al., 2014; Song and Saraswathy, 2007). In contrast, fewer papers can be found on the corrosion of materials that have waste in their formulation. However, this type of study is

* Corresponding author.
E-mail address: almir@ufscar.br (A. Sales).

https://doi.org/10.1016/j.jclepro.2020.124697
0959-6526/

essential in view of the significantly different chemical compositions they present. Therefore, and for the sake of their applicability in the construction industry, it is fundamental to guarantee that bio-concrete also conforms to quality standards in terms of its resistance to corrosion.

In order to further investigate the impact of using SBAS in the mortar formulation, and therefore spot the practical effects of using biomass-containing concrete in civil construction, this paper presents an electrochemical approach to study the durability of carbon steel reinforcements in the presence of SBAS compared to that in a SBAS-free medium. It focused on analysing the initial stages of the passive film formation on carbon steel reinforcements in contact with simulated concrete pore solutions (CPSs) with or without SBAS in their compositions. Electrochemical, physical, and morphological characterisations were performed on both materials. Rather than using mortar as a medium, it performed the analyses using CPSs, which exhibit much lower resistivity and equivalent results compared to those from analyses performed in concrete matrices (Ghods et al., 2009; Lee et al., 2018; Toujas et al., 2017; Yonezawa et al., 1988). In this way, a simpler and faster methodology could be applied to investigate the formation of a passive film on steel, thereby contributing to the current understanding of the impact of the medium on the proneness of rebar to the corrosion process.

2. Experimental

2.1. Test samples

The solution used as simulated CPSs were obtained from the aqueous soluble phase of the dry precursors, which in this case were SBAS-free mortar (fine and coarse sands and cement) and SBAS-containing mortar (fine and coarse sands, SBAS and cement). The resulting CPSs are herein referred to as REF and SBAS, respectively. The cement and natural sand had a 1:3 mass proportion in the reference mortar matrix. In the SBAS-containing mortar precursor, 30% of the natural sand (wt%) was replaced by SBAS, a composition previously demonstrated to provide the resulting concrete with the optimum mechanical and physical features (Almeida et al., 2015).

The cement used was CPV-ARI (Portland cement with a high early strength and a chemical composition (wt%) of 64.0% CaO, 19.2% SiO_2, 5.0% Al_2O_3, 3.2% Fe_2O_3, 2.8% SO_3, 2.4% CO_2, 0.6% MgO, 0.6% K_2O, and 0.1% Na_2O). The SBAS used was standardised by sieving (with a 4.8 mm mesh) and grinding in a ball mill. The resulting chemical composition (wt%) after this process was 91.30% SiO_2, 3.0% Fe_2O_3, 0.5% K_2O, 2.3% Al_2O_3, 0.4% CaO, 0.2% MgO, and 0.9% TiO_2 with a 1.3% loss on ignition. The fine and medium sand employed were both obtained from the São Carlos City area. CPSs were obtained by mixing the mortar matrices with ultra-pure water at a ratio of 3:10 (wt%), followed by mechanical stirring for 24 h (Feng et al., 2017). The resulting supernatant fluids were then filtered and used for the measurements as the concrete pore solutions. Fig. 1 schematically illustrates the process of simulated CPSs obtaining. The ionic conductivities and pHs of these solutions were determined and are listed in Table 1 as mean values, obtained from a triplicate analysis.

2.2. Methods

All of the electrochemical characterisations were performed in a conventional three-electrode glass cell, at 20 °C, using an Autolab-PGSTAT20 potentiostat/galvanostat equipped with an FRA32 module. As the working electrode, a corrugated steel rebar (AISI 1018, Gerdau) typically used in civil construction was cut into

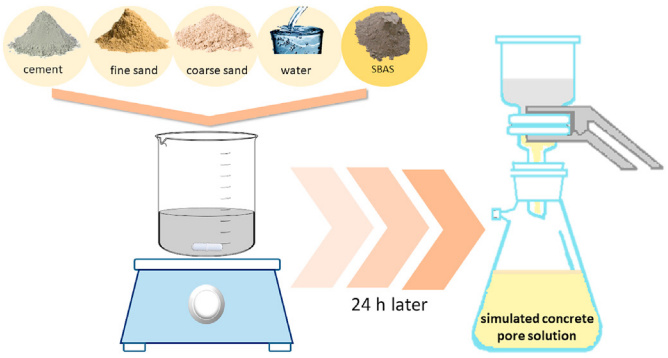

Fig. 1. Schematic representation of the process for obtaining the simulated concrete pore solution.

Table 1
Physical-chemical properties of concrete pore solutions (CPS) obtained.

CPS	pH	Ionic conductivity (mS cm^{-1})
REF	12.49 ± 0.01	11.1 ± 0.2
SBAS	12.44 ± 0.01	10.9 ± 0.2

5 mm-diameter rods and embedded in epoxy resin, leaving an exposed metallic surface of 0.211 cm^2 (geometric area). The chemical composition of the steel used in this work was determined by atomic absorption spectroscopy (Inductar CS cube analyser) as follows: 0.150% C, 0.656% Mn, 0.209% Si, 0.022% P, 0.015% S, and 98.948% Fe. The steel samples were cleaned according to the ASTM standard procedure G1-03 (International, 2017). Prior to the measurements, the working electrode was abraded with sandpaper up to 1200 grit, polished with 0.25 μm alumina, and rinsed with deionised water in an ultrasonic bath. Hg/HgO/KOH (1 mol L^{-1}) was employed as the reference electrode (RE), and a large area Pt wire was used as the auxiliary electrode (AE). The solutions were aerated for 10 min and maintained under an atmospheric air flow during the tests.

The open-circuit potential (OCP) was monitored for 5 consecutive days. Potentiodynamic polarisation tests at 0.5 mV s^{-1} were performed between −200 mV and +1200 mV from the value observed as the OCP, in each case, always starting from the negative and moving toward the positive potential limit. The corrosion current density (j_{cor}) was determined using the method described by McCafferty (Mansfeld, 1976; McCafferty, 2005). The Tafel line of the anodic polarisation curve can be calculated expanding the anodic linear region to potentials below the corrosion potential, and then the anodic current density i_a (net experimental) is calculated from (McCafferty, 2005):

$$i_a(net\ \ experimental) = i_a(experimental) - |i_c(expanded)| \quad (1)$$

The polarisation resistance R_p as determined from the Stern–Geary constant B, can be calculated as follows (Mansfeld, 1976):

$$R_p = \frac{B}{j_{cor}} \quad (2)$$

The pitting potential, E_{pit}, was also determined from the polarisation curves. This was the potential where the current density suddenly increased (pitting initiation) (Shanlin, 2016).

Electrochemical impedance spectroscopy (EIS) was performed at the OCP, in the frequency range of 10 kHz to 10 mHz, applying an AC modulation of 10 mV, and the frequency sampling was 10 points

per decade. All of the EIS spectra were curve-fitted using ZView software.

The *ex situ* characterisation of the working electrode surface immersed in the different CPSs here investigated was also conducted at different immersion periods. The morphology and elemental composition of the passive films formed were investigated using scanning electron microscopy (SEM) coupled to energy dispersive spectrometry (EDS) [Inspect-50, ZEISS]. X-ray diffractograms were obtained using a Rigaku-Rint 2000 diffractometer. X-ray photoelectron spectroscopy (XPS) were performed on spectrometer Scienta Omicron, model ESCA 2SR, with Mg Kα monochromator as the incident photon energy.

3. Results and discussion

3.1. Open-circuit potential evolution profile and potentiodynamic polarisation

The OCP transients, as an important parameter to evaluate the susceptibility to corrosion (Taji et al., 2019), were monitored at regular intervals during the 5 days of the steel samples immersed in the REF and SBAS concrete pore solutions as the CPSs. The responses of a set of two prepared samples of each CPS are shown in Fig. 2A. The mean OCP values recorded for the system in SBAS were found to be approximately 100 mV less negative than in the control sample (REF) during the initial two days of measurements. This observation was also valid for the final two days of measurements, where the difference in the OCP reached as high as 150 mV.

It should be noted that the OCP values measured in both solutions showed dramatic changes for the first 70 h. In the system containing the SBAS solution, a sharp increase in the OCP during the first 5 h (+25 mV h^{-1}) was observed. A rather slower variation of the OCP followed in the subsequent days, at a rate of approximately +4 mV h^{-1}, until it reached a steady-state from the third day on, at +40 mV (*vs.* Hg/HgO/1 M KOH). On the other hand, the data obtained using REF as the electrolyte showed a much steeper increase in the OCP for the initial 66 h, with a rate of approximately +18 mV h^{-1}. Interestingly, in this system, a plateau indicating the apparent stabilisation of the OCP was detected after 48 h of immersion, followed by a steady decrease in the OCP, reaching a rate of less than −0.5 mV h^{-1} in the final monitoring period. Because the OCP presents the tendency of a material to undergo electrochemical reactions with the surrounding medium, a nobler equilibrium OCP value and more stable OCP transient profile indicate a surface that is less susceptible to the corrosion process. In this way, the results suggested that REF was a rather more corrosive medium than SBAS. Despite the fact that no clear indication of the corrosion characteristic of the solution can be inferred from the pH or conductivity values given in Table 1, the OCP monitoring was commonly used to this very end. Overall, the less negative OCP values and the transient profile recorded for the SBAS-containing sample showed the greater susceptibility to the growth of a passivating film on the steel immersed in SBAS compared to that in the REF medium. Thus, the corrosion process was more inhibited in SBAS in comparison to the SBAS-free medium.

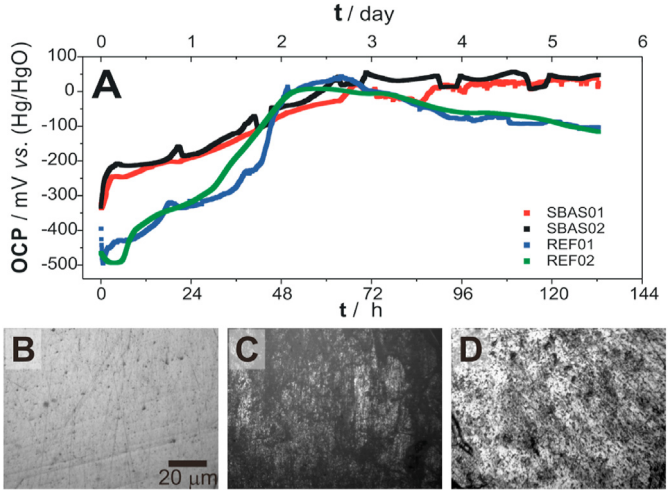

Fig. 2. (A) Evolution of open-circuit potential (OCP) values as function of immersion time of AISI 1018 steel samples in sugarcane bagasse ash sand (SBAS) and reference (REF) simulated concrete pore solutions. Optical micrographs of AISI 1018 steel before (B) and after 5 days of immersion in SBAS (C) and REF (D) solutions.

In addition, light-field optical microscopy images of the working electrode after 5 days are depicted in Fig. 2B–D. Although the results of this qualitative analysis cannot be used to determine the nature of the developed coating films with absolute certainty, it is clear that a more homogenous and opaque film was formed in the SBAS-containing medium compared to the case of the SBAS-free medium, as shown by the comparative analysis results of Fig. 2C and D. Considering the Pourbaix diagram (Refait et al., 1998), it is plausible to expect the film growth to be a result of the formation of iron (hydro)oxides. According to the literature (Zhang and Cheng, 2009), corrosion products on steel are expected to contain both FeOOH and Fe_2O_3. The anodic process is characterised by the dissolution of iron (Wang et al., 2019):

$$Fe \rightarrow Fe^{2+} + 2e^- \quad \text{R1}$$

The iron ions combine with hydroxide ions to form $Fe(OH)_2$ corrosion scales:

$$Fe^{2+} + 2OH^- \rightarrow Fe(OH)_2 \quad \text{R2}$$

$Fe(OH)_2$ can first be oxidised to form FeOOH. Then, because FeOOH is unstable, it oxidises to Fe_2O_3 in the presence of oxygen, as described by R3 and R4:

$$2\ Fe(OH)_2 + {}^1/_2O_2 \rightarrow 2\ FeOOH + H_2O \quad \text{R3}$$

$$2\ FeOOH \rightarrow Fe_2O_3 + H_2O \quad \text{R4}$$

On the other hand, a cathodic reaction in a neutral or an alkaline medium is dominated by the reduction of oxygen (Wang et al., 2019; Zhang and Cheng, 2009):

$$O_2 + 2H_2O + 4e^- \rightarrow 4OH^- \quad \text{R5}$$

In order to further investigate an initial hypothesis that the REF and SBAS medium showed different passivating natures, linear sweep voltammetry was performed at the initial and final periods of measurement (0 and 5 days). The resulting comparison between the systems based on these polarisation curves is presented in Fig. 3. The most important parameters measured from these curves are summarised in Table 2.

Regarding the corrosion potential, E_{cor}, less negative values were obtained for the system in SBAS than in the case of the REF medium. However, the difference in E_{cor} between the two freshly immersed electrodes in the pore solution was relatively low, at approximately 47 mV. After 5 days, the scenario was somewhat altered, and the E_{cor} values detected in the two medium were more distinct, at +34 and −121 mV in the SBAS and REF medium, respectively. The difference in E_{cor} was 155 mV. This higher value could indicate that when the immersion time increased for the sample immersed in

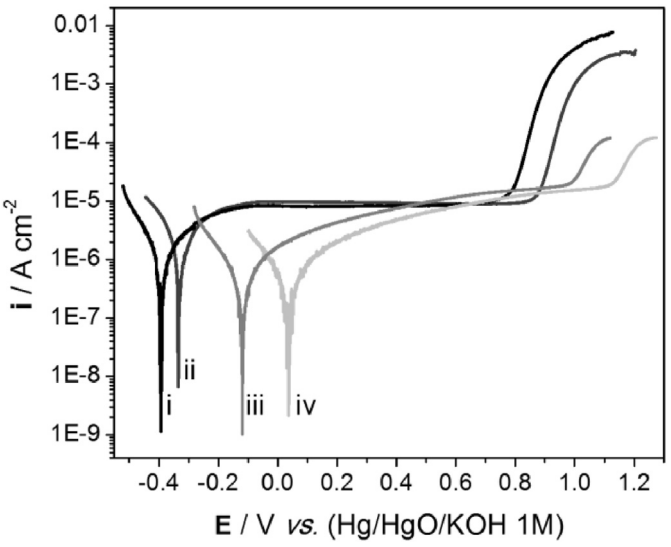

Fig. 3. Polarisation curves obtained in REF (i, iii) and SBAS (ii, iv) medium right after immersion of working electrode (curves i and ii) and after 5 days of immersion (curves iii and iv).

film on the steel surface (Tang et al., 2013). On the other hand, |Z| increased by less than two times for the electrode immersed in the REF solution and reached just 469 Ω cm^2 at 125 Hz. The values found in the SBAS solution are an additional indication that the SBAS medium might favour passive film formation in comparison to the control medium, REF.

Different equivalent electric circuit models have been used to interpret impedance spectra on passive and active metal surfaces (Arzola and Genescá, 2005; Cao et al., 2017; Feng et al., 2017; Jiang et al., 2017; Tang et al., 2013; Ye et al., 2013). Thus, because a passive film formed on the steel reinforcement surface and electrochemical reactions occurred at the metal/film interface, the equivalent circuit, as shown in Fig. 5, was the most appropriated to explain the physical phenomena expressed by the experimental data (Liu et al., 2017, 2019), as shown in the fitting curves of Fig. 4. The high-frequency time constant is represented by the solution resistance (R_{sol}), the passive layer resistance (R_{film}) with constant-phase elements (CPE) associated to passive film capacitance (Q_{film}). The low frequency time constant is represented by the charge transfer resistance (R_{ct}) and to double layer capacitance (Q_{dl}). Note that in the equivalent electrical circuit, CPE were used instead of pure capacitors in order to take into account the inhomogeneity present at

Table 2
Tafel data obtained from polarisation curves shown in Fig. 3.

Medium	E_{cor}/mV *vs.* (Hg/HgO/KOH 1 M)	j_{cor}/μA cm^{-2}	R_p/kΩ cm^2	E_{pit}/*V vs.* (Hg/HgO/KOH 1 M)
REF (fresh)	−395	2.11	1.3	+0.780
SBAS (fresh)	−332	2.05	0.8	+0.839
REF (after 5 days)	−121	1.14	15	+0.985
SBAS (after 5 days)	+34	0.37	26	+1.130

the SBAS solution, the corrosion process decreased. It was also observed that the pitting potential (E_{pit}) had the same behaviour as E_{cor}. Thus, after five days of immersion in the SBAS solution, E_{pit} shifted by +310 mV. On the other side, to the REF solution E_{pit} was only displaced by +200 mV. These results corroborate the results of the OCP transient analysis previously shown in Fig. 2A. Moreover, the obtained corrosion current densities (J_{cor}) and polarisation resistances (R_p) reveal a lower corrosion rate and greater resistive characteristic, respectively in the SBAS medium compared to those in the REF medium, which reinforces the hypothesis of the promoted formation of a passive film in the SBAS-containing medium. Because R_p is commonly used as a measure of a metal's resistance to corrosion damage, high values of R_p are associated with a high corrosion prevention ability, whereas low values of R_p indicate high corrosion activity (Lu and Ba, 2010).

3.2. Electrochemical impedance spectroscopy

Aiming at a better understanding of the growth and physical differences between the passivating films formed, EIS experiments were carried out at the OCP value during different monitoring days (0, 1, 2, 3, 4, and 5 days). Fig. 4 shows representative EIS diagrams for both simulated solutions at different monitoring days. The Nyquist plots show an increase in the diameter of the capacitive loop in both the SBAS and REF solutions with time. This is a typical aspect observed when surfaces become more oxidised, confirming that a passivation process is taking place. After 5 days of immersion, the impedance magnitude (|Z|) for the electrode immersed in the SBAS solution reached 867 Ω cm^2 at 125 Hz. This value was more than three times the value obtained at 0 days in the same solution (270 Ω cm^2). This increase is attributed to the formation of a passive

the reinforcement/simulated pore solution interface (Liu et al., 2019; Omanovic and Roscoe, 2000). Furthermore, this analysis of the proposed electrical circuit yielded fitted data with absolute errors below 10% for all parameters.

From the data obtained from CPE, it is possible to estimate the values of the apparent capacitance of passive films/corrosion products (C_{film}) and the apparent capacitance of the double layer (C_{dl}), as described at (Liu et al., 2017; Ma et al., 2000; Shi et al., 2018). Fig. 6 shows a comparison of the electrochemical parameters calculated for the SBAS and REF solutions. The trends observed for parameters R_{ct} and C_{dl} are indeed similar in the SBAS and REF solutions, although the absolute values differ considerably. Clearly, the film resistance (R_{film}) increased until the 3rd day in the SBAS solution and until the 4th day in the REF solution. The charge transfer resistance (R_{ct}) increased in both solutions until the 4th day. However, higher resistance values are observed for the data obtained in the SBAS solution. According to the fitted results shown in Fig. 6BD and , almost no variation was detected in the capacitances. Nonetheless, it is worth remembering that this value depends on the morphology of the film and its thickness (Fattah-alhosseini and Vafaeian, 2015; Shi et al., 2018). These results are in agreement with the literature (Feng et al., 2017; Ghods et al., 2009; Jiang et al., 2017; Kim and Young, 2013) and consistent with the potentiodynamic polarisation results. More importantly, R_{ct} increased with the immersion time for the sample immersed in SBAS. In contrast, a lower variation for these values is found in the data obtained in REF. The latter indicates that the passive film becomes more protective with an increase in either the time or passivation potential (Kim and Young, 2013). This more complete analysis further confirms that the film obtained in the SBAS solution had better passivating properties than that obtained in the REF

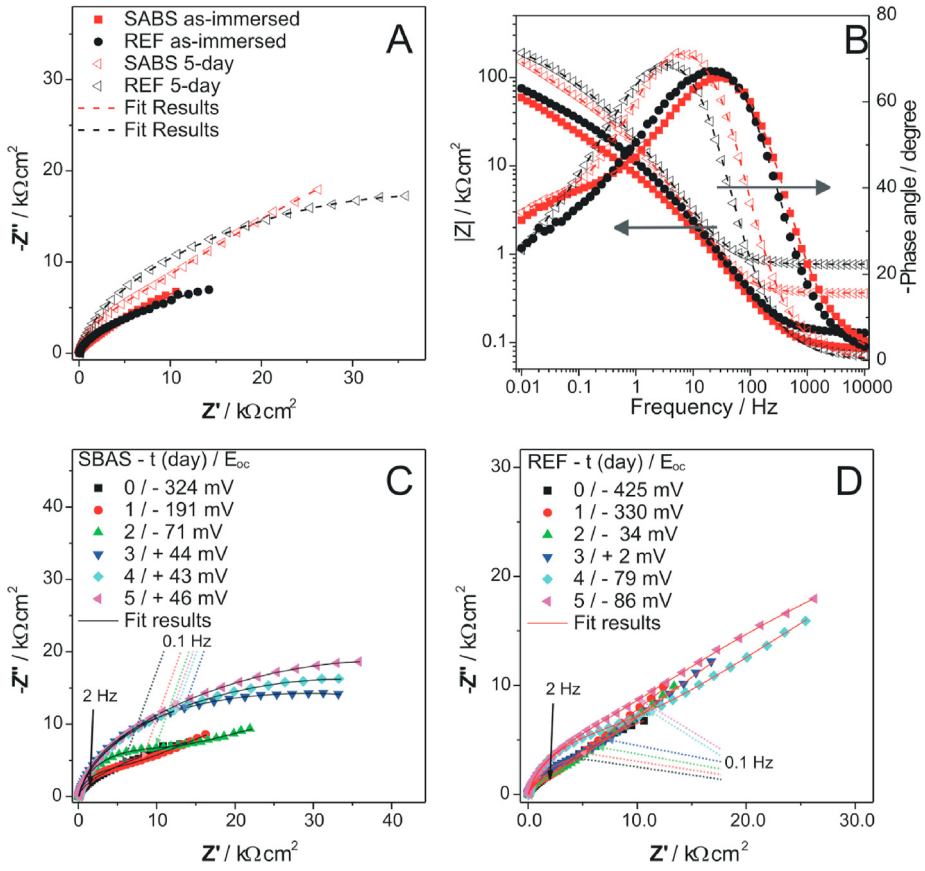

Fig. 4. (A) Nyquist plot obtained just after immersion (closed symbols) and after (opened symbols) 5 days of immersion in SBAS (red) and REF (black) solutions. (B) Bode diagram obtained in SBAS (black curves) and REF solutions (red curves) at different immersion times: as-immersed (closed symbols) and after 5 days (opened symbols). Complete time-dependent Nyquist plots of the EIS response recorded at E_{oc} in (C) SBAS and (D) REF solutions. (For interpretation of the references to colour in this figure legend, the reader is referred to the Web version of this article.)

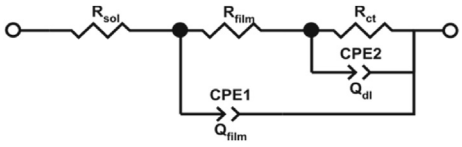

Fig. 5. Equivalent electrical circuits proposed to fit impedance spectra.

solution, suggesting that SBAS acted analogously to a corrosion inhibitor additive.

As the main result, the passive film formed in the SBAS solution showed higher stability and less susceptibility to corrosion. Consequently, it is expected the addition of SBAS to the concrete composition prevent the pitting corrosion of the steel, which is the most common corrosion process that takes place in such environments (Yonezawa et al., 1988).

3.3. Steel morphological characterisation

By means of scanning electron microscopy, the working electrode surface was investigated to characterise the passive films formed during 5 consecutive days of immersion in the REF and SBAS medium. A representative set of micrographs are depicted in Fig. 7.

Passivation products are already visible in Fig. 7A and E. Note that the defects formed by the polishing process, as seen on the fresh surface shown in the insets, become undetectable. Rod-shaped precipitates are clearly observed in Fig. 7B and F, which seem to grow at the edge when the amount of precipitate increases with the immersion time, leading to a globular-like structure, from the third day on (Fig. 7C and G). As seen in the micrographs, the steel surface immersed in the SBAS medium shows a higher total coverage than that in the REF medium. This behaviour is more evident by the final monitoring period (Fig. 7D: SBAS; Fig. 7H: REF), where a completely covered surface is found in Fig. 7D.

A possible explanation for the formation of the precipitate comes from the local pH variation at the steel/solution interface level. It is well-known that the formation of passive films (iron oxy-hydroxides) promotes a local decrease in pH, causing a pH shift as high as 3 units according to some authors (da Silva et al., 2016). In solutions containing high amounts of calcium hydroxides, which is indeed the case with the CPS solutions here investigated, an important decrease in the $CaCO_3$ solubility could reasonably explain the precipitation of such compounds on the steel being passivated.

To identify the chemical nature of such precipitates, chemical mapping was performed using energy dispersive X-ray spectroscopy. In addition, X-ray diffraction (XRD) analyses of the samples immersed in SBAS and REF solutions were performed. The results of both analyses are shown in Fig. 8.

Although only the mapping performed for the samples after 1 day of immersion in the SBAS medium was showed, it is enough to reveal the presence of Ca and O, and more importantly, the absence of iron in the aggregates (Fig. 8A), supporting the previous statement that the majority of the precipitate is calcium carbonate

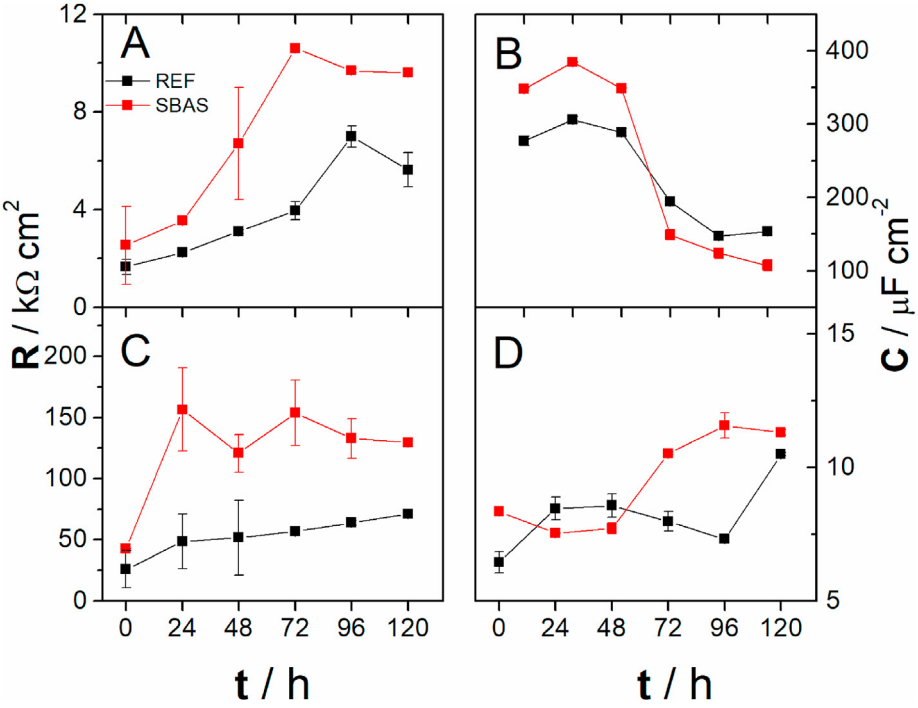

Fig. 6. Fitted electrochemical impedance data obtained for REF (black) and SBAS (red) solutions during passivation stages: (A) R_{film}, (B) C_{film}, (C) R_{ct}, and (D) C_{dl}. (For interpretation of the references to colour in this figure legend, the reader is referred to the Web version of this article.)

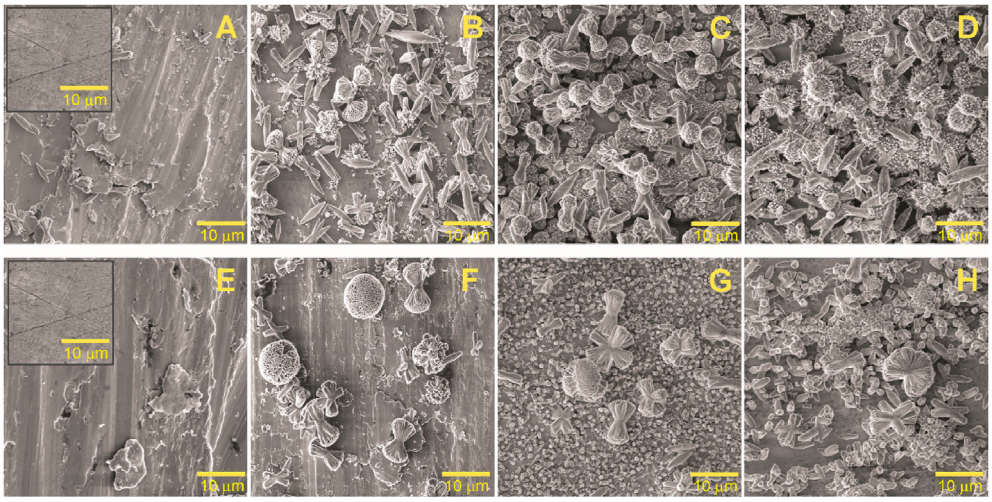

Fig. 7. SEM images of working electrode surfaces after different numbers of days of immersion (1 day: A-B and E-F, 3 days: C and G, and 5 days: D and H) in SBAS solution (A–D) and in REF solution (E–H), inset: fresh and polished AISI 1018 steel surface.

($CaCO_{3(s)}$). It is also possible to note that oxygen is distributed all over the electrode surface, with some dark areas correlated with the absence of iron.

The presence of oxygen on the entire surface is expected, once iron oxy-hydroxide is formed as the main passivating agent in the current investigation. In the obtained diffractograms, it was not possible to detect peaks related to iron oxy-hydroxides phases. There could be various reasons for this, including the following: i) the film is amorphous or nanocrystalline, or ii) the film is too thin and the XRD technique becomes pointless for this purpose. However, the results allowed us to detect $CaCO_3$ patterns in both samples. In addition, these outcomes highlight that the ratio of the peaks associated with calcium is higher for the sample immersed in the SBAS solution than that in REF, which might be attributed to the formation of a thicker film in this medium once the precipitation depends on the local pH variation, with a greater passive film growth associated with a greater pH variation. Consequently, there will be a greater precipitation of $CaCO_3$ on the surface of the metal.

For a better characterisation of the passive film formation, XPS measurements were performed for the samples after 5 days of immersion in REF and SABS medium solutions. The long scans are shown in Fig. 9. Only iron, oxygen, carbon, silicon and calcium were detected for both samples, showing no contamination of the formed films. Fig. 10 presents the XPS spectra for Fe $2p_{3/2}$ and O 1s regions. In the Fe $2p_{3/2}$ spectra, three species were observed: metallic Fe (706.9 ± 0.1eV), Fe^{2+} (709.7 ± 0.1eV) and Fe^{3+}

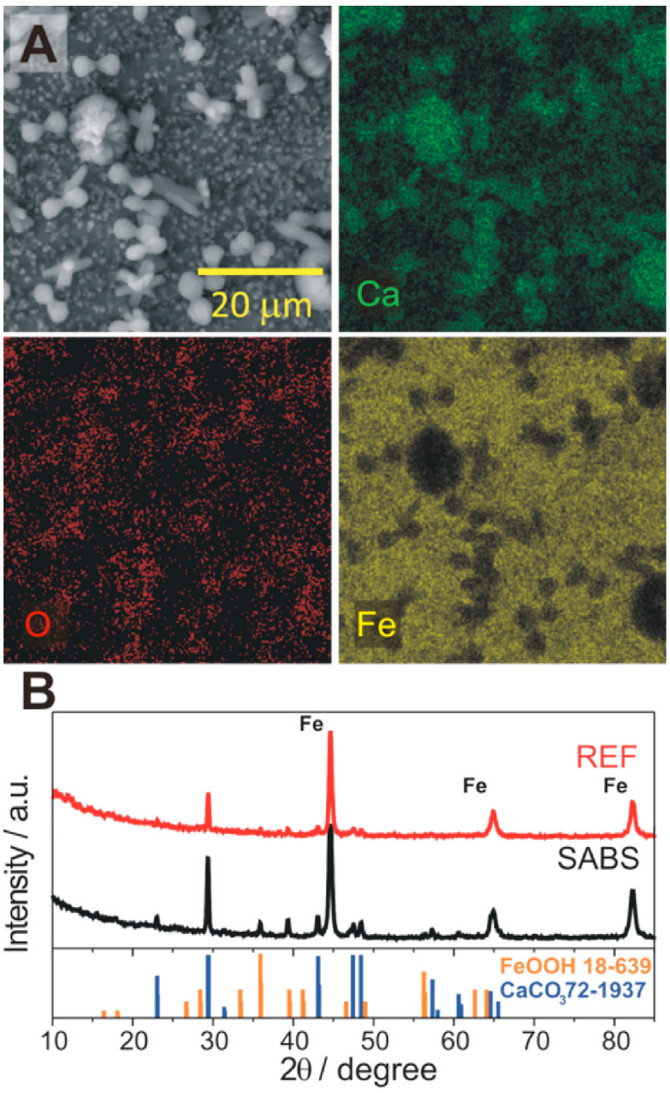

Fig. 8. (A) FE-SEM with elemental mapping (Ca, O, Fe) of steel surface after 5 days of immersion in SBAS-containing solution. (B) XRD data after 5 days of immersion in SBAS (black) and REF (red) solutions. (For interpretation of the references to colour in this figure legend, the reader is referred to the Web version of this article.)

(711.2 ± 0.1eV), (Ghods et al., 2012; Shi et al., 2020; Wang et al., 2020). The peak observed in 713.2 ± 0.2 eV corresponds to a Fe^{2+} satellite (Wang et al., 2020). In O 1s spectra, two species were identified: O^{2-} (530.0 ± 0.1eV) and OH^- (531.6 ± 0.2 eV), which are related to the lattice oxygen and hydroxy groups in FeOOH and/or $Fe(OH)_3$ compounds, respectively (Shi et al., 2020; Wang et al., 2020). The ratios of O^{2-}/OH^- and Fe^{2+}/Fe^{3+} species in the passive film were calculated, based on the XPS spectra, and the results are shown in Fig. 11. The increasing of the O^{2-}/OH^- and Fe^{2+}/Fe^{3+} ratios is usually attributed to an inhibition of iron oxidation, due the possible formation of a spinel structure, such as Fe_3O_4 from Fe^{2+} species (Asami et al., 1976; Shi et al., 2020), while hydroxide species are observed in rebar corrosion (Wang et al., 2020). In the films formed from REF and SBAS, similar ratios of Fe^{2+}/Fe^{3+} species were observed. However, the highest relative content of O^{2-}/OH^- ratio on the SBAS film corroborates the finding that the film obtained from SBAS is more protective than the one formed in the REF solution.

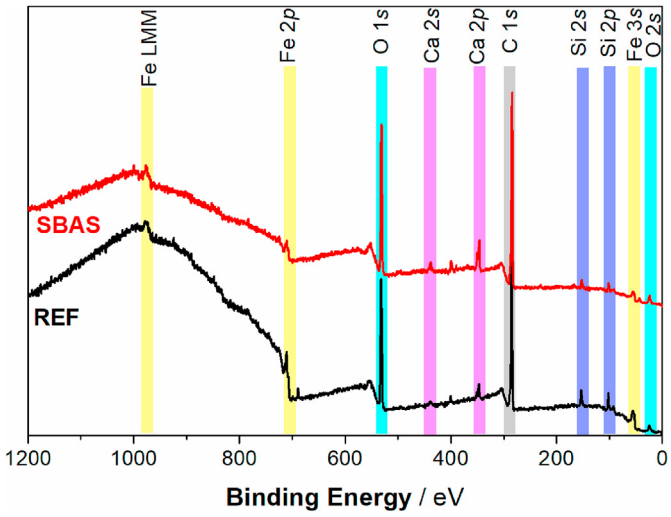

Fig. 9. Long scan of XPS spectra for the passive films formed after immersion in REF and SBAS solutions for 5 d.

4. Conclusions

Herein, this paper presented the results of an investigation of the impact of adding SBAS to mortar on the proneness of steel to corrosion. Concrete pore solutions were used, and electrochemical and morphological examinations were performed. In light of the results shown, the following conclusions were drawn:

- According to the OCP and potentiodynamic profiles, a passive film grew faster on a steel surface immersed in the SBAS-containing solution than in the control sample, REF, indicating that SBAS could function as a corrosion inhibitor.
- Although the films presented very similar morphologies, data obtained from EIS reinforced that the passivating films obtained in the SBAS medium had better passivating properties.
- The chemical mapping of the precipitates found at the steel surface corroborated the idea of calcium hydroxides being formed.

Overall, this study showed that replacing natural fine sand with SBAS in a concrete formulation has potential benefits in relation to its passivating properties, *i.e.* SBAS-containing concrete seems to be a less aggressive medium for steel. The lower susceptibility to steel corrosion in the SBAS medium is here attributed to the faster passivating characteristic of the SBAS medium, based on the monitoring of different electrochemical parameters and additional morphological characterisation.

Data availability statement

The raw/processed data required to reproduce these findings will be made available on request.

CRediT authorship contribution statement

Murilo F. Gromboni: Investigation, Methodology, Data curation, Writing - original draft, preparation. **Almir Sales:** Conceptualization, Supervision, Writing - review & editing, Project administration, Resources. **Mariana de A.M. Rezende:** Investigation, Methodology, Data curation, Writing - original draft, preparation. **Juliana P. Moretti:** Investigation, Methodology, Writing - original draft, preparation. **Patricia G. Corradini:** Writing - review &

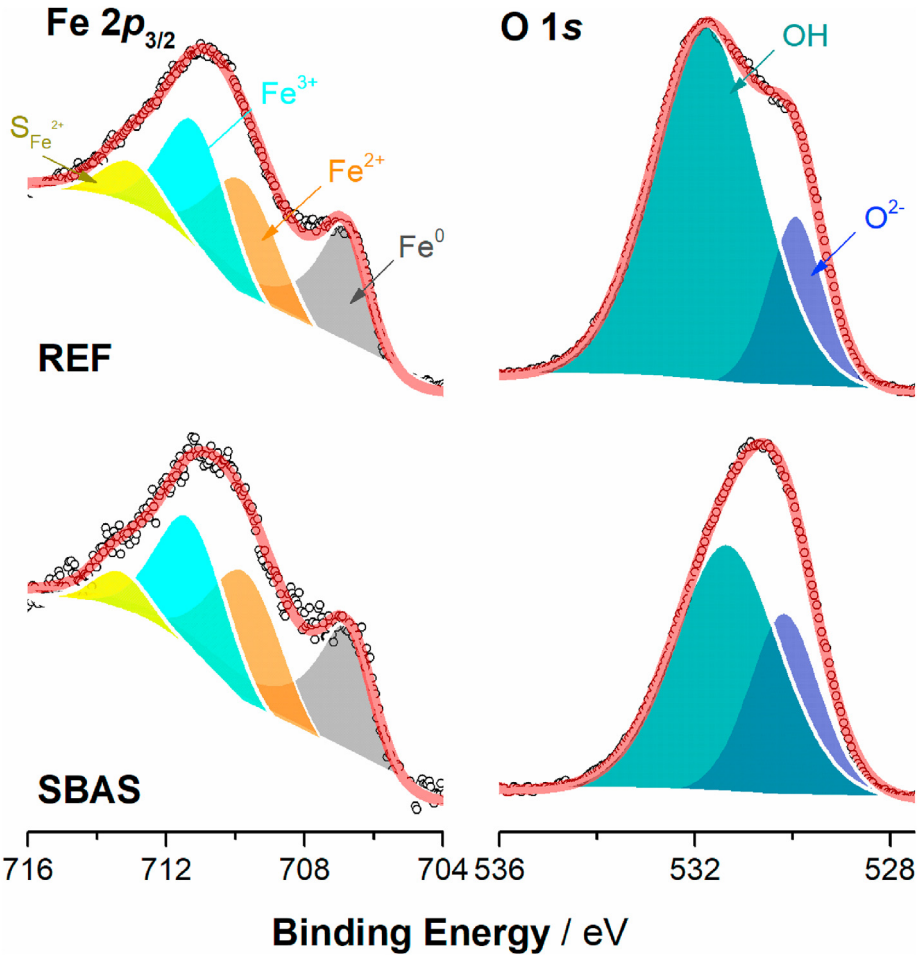

Fig. 10. X-ray photoelectron spectra in Fe $2p_{3/2}$ and O 1*s* regions after immersion in REF and SBAS solutions for 5 d.

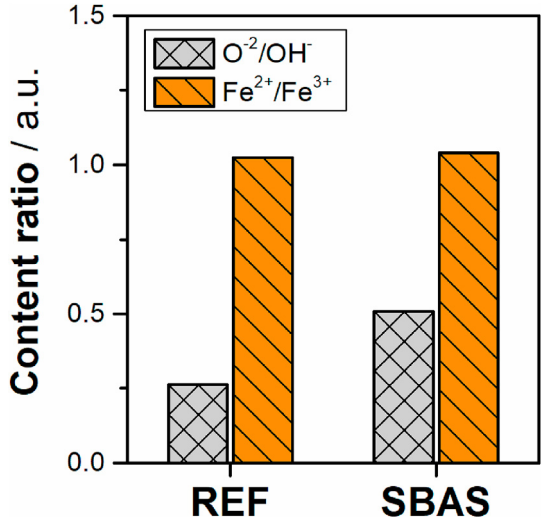

Fig. 11. O^{2-}/OH^{-} and Fe^{2+}/Fe^{3+} ratios obtained by XPS measurements of passive films formed after immersion in REF and SBAS solutions for 5 d.

editing. **Lucia H. Mascaro:** Visualization, Supervision, Writing - review & editing, Resources.

Declaration of competing interest

The authors declare that they have no known competing financial interests or personal relationships that could have appeared to influence the work reported in this paper.

Acknowledgements

The authors express gratitude to Professor Valmor Mastelato, for the XPS measures and also thank the Sao Paulo Research Foundation (FAPESP) for the grant received [#2013/07296-2], along with Coordenação de Aperfeiçoamento de Pessoal de Nível Superior (CAPES) [Finance Code001] and MCTI / CNPq for their financial support [grants # 309892/2013-9 and #150481/2017-9].

References

Ahmad, S., 2003. Reinforcement corrosion in concrete structures, its monitoring and service life prediction––a review. Cement Concr. Compos. 25 (4), 459–471.
Almeida, F.C.R., Sales, A., Moretti, J.P., Mendes, P.C.D., 2015. Sugarcane bagasse ash sand (SBAS): Brazilian agroindustrial by-product for use in mortar. Construct. Build. Mater. 82, 31–38.
Anupam, A.K., Kumar, P., G.D. Ransinchung, R.N., 2013. Use of various agricultural and industrial waste materials in road construction. Procedia - Social and Behavioral Sciences 104, 264–273.
Arzola, S., Genescá, J., 2005. The effect of H2S concentration on the corrosion behavior of API 5L X-70 steel. J. Solid State Electrochem. 9 (4), 197–200.
Asami, K., Hashimoto, K., Shimodaira, S., 1976. An ESCA study of the Fe2+/Fe3+ ratio in passive films on iron-chromium alloys. Corrosion Sci. 16 (6), 387–391.
Cao, Y., Dong, S., Zheng, D., Wang, J., Zhang, X., Du, R., Song, G., Lin, C., 2017.

Multifunctional inhibition based on layered double hydroxides to comprehensively control corrosion of carbon steel in concrete. Corrosion Sci. 126, 166–179.
da Silva, M.M., Mascaro, L.H., Pereira, E.C., Zimer, A.M., 2016. Near-surface solution pH measurements during the pitting corrosion of AISI 1020 steel using a ring-shaped sensor. J. Electroanal. Chem. 780, 379–385.
de Souza, Z.J., 2017. Dois leilões de energia elétrica para fazer girar a roda. unica.com.br/colunas/17601337920328608058/em-2017-por-cento2C-dois-leiloes-de-energia-eletrica. (Accessed 4 February 2018).
Farias, J.M.B.A., Costa, F.S., 2018. Acompanhamento da Safra Brasileira de Cana-de-açúcar. In: Companhia Nacional de Abastecimento, C. (Ed.), Superintendência de Administração. Brasil.
Fattah-alhosseini, A., Vafaeian, S., 2015. Passivation behavior of a ferritic stainless steel in concentrated alkaline solutions. J Mater Res Technol 4 (4), 423–428.
Feng, X., Shi, R., Lu, X., Xu, Y., Huang, X., Chen, D., 2017. The corrosion inhibition efficiency of aluminum tripolyphosphate on carbon steel in carbonated concrete pore solution. Corrosion Sci. 124, 150–159.
Ghods, P., Burkan Isgor, O., Bensebaa, F., Kingston, D., 2012. Angle-resolved XPS study of carbon steel passivity and chloride-induced depassivation in simulated concrete pore solution. Corrosion Sci. 58, 159–167.
Ghods, P., Isgor, O.B., McRae, G., Miller, T., 2009. The effect of concrete pore solution composition on the quality of passive oxide films on black steel reinforcement. Cement Concr. Compos. 31 (1), 2–11.
Hornbostel, K., Larsen, C.K., Geiker, M.R., 2013. Relationship between concrete resistivity and corrosion rate – a literature review. Cement Concr. Compos. 39, 60–72.
International, A., 2017. G1 - 03(2017)e1 - Standard Practice for Preparing, Cleaning, and Evaluating Corrosion Test Specimens, Methods for Preparing Specimens for Test. West Conshohocken, PA.
Jiang, J.-y., Wang, D., Chu, H.-y., Ma, H., Liu, Y., Gao, Y., Shi, J., Sun, W., 2017. The passive film growth mechanism of new corrosion-resistant steel rebar in simulated concrete pore solution: nanometer structure and electrochemical study. Materials 10 (4), 412.
Kim, J.J., Young, Y.M., 2013. Study on the passive film of type 316 stainless steel. Int. J. Electrochem. Sci. 8 (8), 11847–11859.
Lee, H.S., Yang, H.M., Singh, J.K., Prasad, S.K., Yoo, B., 2018. Corrosion mitigation of steel rebars in chloride contaminated concrete pore solution using inhibitor: an electrochemical investigation. Construct. Build. Mater. 173, 443–451.
Lima, S.A., Sales, A., Almeida, F.d.C.R., Moretti, J.P., Portella, K.F., 2011. Concretos com cinza do bagaço da cana-de-açúcar: avaliação da durabilidade por meio de ensaios de carbonatação e abrasão. Ambiente Construído 11, 201–212.
Liu, G.J., Zhang, Y.S., Wu, M., Huang, R., 2017. Study of depassivation of carbon steel in simulated concrete pore solution using different equivalent circuits. Construct. Build. Mater. 157, 357–362.
Liu, R., Jiang, L.H., Xu, J.X., Xiong, C.S., Song, Z.J., 2014. Influence of carbonation on chloride-induced reinforcement corrosion in simulated concrete pore solutions. Construct. Build. Mater. 56, 16–20.
Liu, Y., Song, Z., Wang, W., Jiang, L., Zhang, Y., Guo, M., Song, F., Xu, N., 2019. Effect of ginger extract as green inhibitor on chloride-induced corrosion of carbon steel in simulated concrete pore solutions. J. Clean. Prod. 214, 298–307.
Lu, S., Ba, H.-J., 2010. Corrosion sensor for monitoring the service condition of chloride-contaminated cement mortar. Sensors 10 (4), 4145.
Ma, H., Cheng, X., Li, G., Chen, S., Quan, Z., Zhao, S., Niu, L., 2000. The influence of hydrogen sulfide on corrosion of iron under different conditions. Corrosion Sci. 42 (10), 1669–1683.
Mansfeld, F., 1976. The polarization resistance technique for measuring corrosion currents. In: Fontana, M.G., Staehle, R.W. (Eds.), Advances in Corrosion Science and Technology, vol. 6. Springer US, Boston, MA, pp. 163–262.
McCafferty, E., 2005. Validation of corrosion rates measured by the Tafel extrapolation method. Corrosion Sci. 47 (12), 3202–3215.
Moretti, J.P., Sales, A., Almeida, F.C.R., Rezende, M.A.M., Gromboni, P.P., 2016. Joint use of construction waste (CW) and sugarcane bagasse ash sand (SBAS) in concrete. Construct. Build. Mater. 113, 317–323.
Moretti, J.P., Sales, A., Quarcioni, V.A., Silva, D.C.B., Oliveira, M.C.B., Pinto, N.S., Ramos, L.W.S.L., 2018. Pore size distribution of mortars produced with agro-industrial waste. J. Clean. Prod. 187, 473–484.
Omanovic, S., Roscoe, S.G., 2000. Interfacial behavior of beta-lactoglobulin at a stainless steel surface: an electrochemical impedance spectroscopy study. J. Colloid Interface Sci. 227 (2), 452–460.
Ozório, M.d.S., Reis, E.A.P.d., Teixeira, S.R., Bellucci, F.S., Job, A.E., 2015. Sugarcane bagasse ash as a reinforcing filler in thermoplastic elastomers: structural and mechanical characterizations. J. Appl. Polym. Sci. 132 (7).
Refait, P.H., Abdelmoula, M., GÉnin, J.M.R., 1998. Mechanisms of formation and structure of green rust one in aqueous corrosion of iron in the presence of chloride ions. Corrosion Sci. 40 (9), 1547–1560.
Santos, R.J.d., Agostini, D.L.d.S., Cabrera, F.C., Reis, E.A.P.d., Ruiz, M.R., Budemberg, E.R., Teixeira, S.R., Job, A.E., 2014. Sugarcane bagasse ash: new filler to natural rubber composite. Polímeros 24, 646–653.
Shanlin, W., 2016. Corrosion resistance and electrocatalytic properties of metallic glasses. In: Movahedi, B. (Ed.), Metallic Glasses. IntechOpen.
Shi, J., Ming, J., Sun, W., 2018. Electrochemical performance of reinforcing steel in alkali-activated slag extract in the presence of chlorides. Corrosion Sci. 133, 288–299.
Shi, J., Ming, J., Wang, D., Wu, M., 2020. Improved corrosion resistance of a new 6% Cr steel in simulated concrete pore solution contaminated by chlorides. Corrosion Sci. 174, 108851.
Song, H.-W., Saraswathy, V., 2007. Corrosion monitoring of reinforced concrete structures - a review. Int. J. Electrochem. Sci. 2, 1–28.
Taji, I., Ghorbani, S., de Brito, J., Tam, V.W.Y., Sharifi, S., Davoodi, A., Tavakkolizadeh, M., 2019. Application of statistical analysis to evaluate the corrosion resistance of steel rebars embedded in concrete with marble and granite waste dust. J. Clean. Prod. 210, 837–846.
Tang, F., Cheng, X., Chen, G., Brow, R.K., Volz, J.S., Koenigstein, M.L., 2013. Electrochemical behavior of enamel-coated carbon steel in simulated concrete pore water solution with various chloride concentrations. Electrochim. Acta 92, 36–46.
Toujas, S., Vázquez, M., Valcarce, M.B., 2017. Unexpected effect of citrate ions on the corrosion process of carbon steel in alkaline solutions. Corrosion Sci. 128, 94–99.
Usda, 2017. Sugar: World Markets and Trade Record Global Production Spurs Record Consumption. United States Department of Agriculture, p. 8.
Wang, C., Chen, J., Hu, B., Liu, Z., Wang, C., Han, J., Su, M., Li, Y., Li, C., 2019. Modified chitosan-oligosaccharide and sodium silicate as efficient sustainable inhibitor for carbon steel against chloride-induced corrosion. J. Clean. Prod. 238, 117823.
Wang, D., Ming, J., Shi, J., 2020. Enhanced corrosion resistance of rebar in carbonated concrete pore solutions by Na2HPO4 and benzotriazole. Corrosion Sci. 174, 108830.
Ye, C.-Q., Hu, R.-G., Dong, S.-G., Zhang, X.-J., Hou, R.-Q., Du, R.-G., Lin, C.-J., Pan, J.-S., 2013. EIS analysis on chloride-induced corrosion behavior of reinforcement steel in simulated carbonated concrete pore solutions. J. Electroanal. Chem. 688, 275–281.
Yonezawa, T., Ashworth, V., Procter, R.P.M., 1988. Pore solution composition and chloride effects on the corrosion of steel in concrete. Corrosion 44 (7), 489–499.
Zhang, G.A., Cheng, Y.F., 2009. Electrochemical corrosion of X65 pipe steel in oil/water emulsion. Corrosion Sci. 51 (4), 901–907.